nature biomedical engineering

Article

https://doi.org/10.1038/s41551-025-01597-0

Digital CRISPR-based diagnostics for quantification of *Candida auris* and resistance mutations

Received: 29 July 2024

Accepted: 2 December 2025

Published online: 14 January 2026

Check for updates

Justin C. Rolando[1,2,3,11], Anton Thieme[2,3,11], Nicole E. Weckman[2,3,9,11], Nayoung Kim[2,3,4,5], Helena de Puig[2,4,5], Xiao Tan[2,3,4,6], Emily Cotnoir[7], Vishnu Chaturvedi[7,10], James J. Collins[2,4,5,8,12] ✉ & David R. Walt[1,2,3,12] ✉

Candida auris, an increasingly prevalent fungal pathogen, requires both rapid identification and antifungal susceptibility testing to enable proper treatment. This study introduces digital SHERLOCK (dSHERLOCK), a platform that combines CRISPR/Cas nucleic acid detection, single-template quantification and real-time kinetics monitoring. Assays implemented on this platform display excellent sensitivity to *C. auris* from major clades 1–4, while maintaining specificity when challenged with common environmental and pathogenic fungi. dSHERLOCK detects *C. auris* within 20 min in minimally processed swab samples and achieves sensitive quantification (1 c.f.u. μl^{-1}) within 40 min. To address antifungal susceptibility testing, we develop assays that detect mutations that are commonly associated with azole and echinocandin multidrug resistance. We use machine learning and real-time monitoring of reaction kinetics to achieve highly accurate simultaneous quantification of mutant and wild-type *FKS1* SNP alleles in fungal populations with mixed antifungal susceptibility, which would be misdiagnosed as completely susceptible or resistant under standard reaction conditions. Our platform's use of commercially available materials and common laboratory equipment makes *C. auris* diagnostics widely deployable in global healthcare settings.

Candida auris (*C. auris*) is a critical emerging fungal pathogen that has caused outbreaks with high mortality rates in healthcare facilities around the world[1–3]. Its ability to survive on physical surfaces for prolonged durations demands rapid detection for effective outbreak control. Efficient assessment of antifungal resistance is critical to guide fast decisions on patient treatment. In the United States, 90% of all *C. auris* isolates show resistance to azole antifungals, while resistance to the preferred echinocandin antifungal treatments is increasing[4]. Current diagnostic pathways for detecting *C. auris* and its drug susceptibility use a combination of matrix-assisted laser desorption ionization time-of-flight (MALDI-TOF) mass spectrometry, quantitative PCR (qPCR) or culture-based approaches in centralized laboratories[5,6]. These methods are costly, slow and require complex dedicated equipment and trained personnel, all of which impede efficient clinical response[7–9]. There is a need for novel tests to diagnose *C. auris* to allow accurate quantitation of fungal burden and assessment of antifungal resistance[5,6,10].

CRISPR-based diagnostics have emerged as tools to detect nucleic acids[11–14]. CRISPR-based diagnostics are isothermal, fast, easy to use and highly adaptable for field deployment including lyophilised, shelf-stable fluorescent or paper-based formats[15,16]. The isothermal nucleic acid pre-amplification step in nearly all CRISPR-based diagnostics published thus far is essential for maximizing sensitivity[14]. However, continuous amplification limits the ability to accurately

A full list of affiliations appears at the end of the paper. ✉e-mail: jimjc@mit.edu; dwalt@bwh.harvard.edu

https://doi.org/10.1038/s41551-025-01597-0

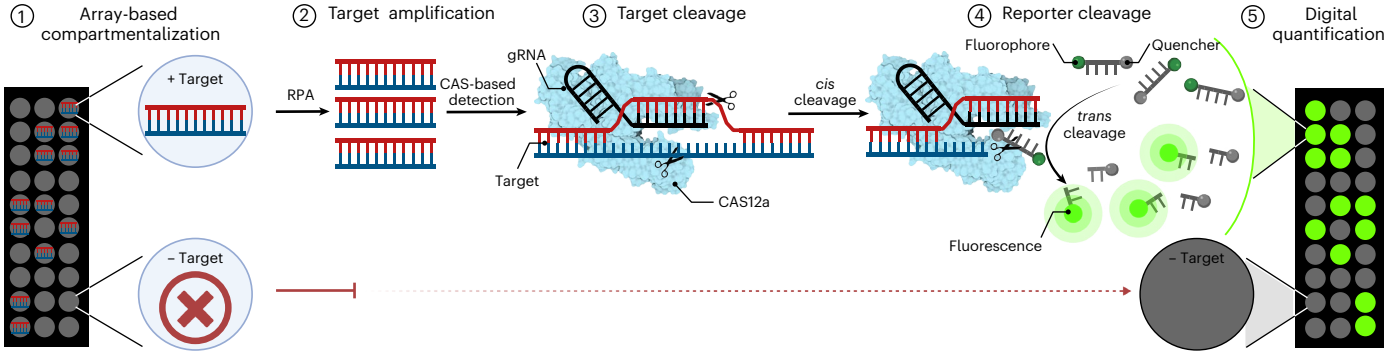


Fig. 1 | Schematic representation of digital SHERLOCK assays. 1. Fluid containing all reagents is distributed into an array of compartments. Each compartment includes the components for RPA and multiple copies of CAS12a ribonuclear-protein complex (Supplementary Table 1). The target analyte is loaded in a binary (presence/absence) fashion that can be described by a Poisson distribution. For a detailed description of the loading procedure, see Methods and Supplementary Fig. 1. **2.** In compartments containing the target template, RPA generates multiple copies of the target amplicons. **3.** Cas12a recognizes the amplified target through hybridization with the complementary guide RNA (gRNA), which subsequently activates *cis* cleavage of both target strands. **4.** Activated Cas12a induces non-specific collateral *trans* cleavage of nearby reporter molecules containing a fluorophore and quencher pair. **5.** Separation of the fluorophore and quencher generates a fluorescent signal, which is followed over time to generate amplification curves. Quantification occurs either 'digitally', where compartments are classified as either 'positive' (signal present) or 'negative' (signal absent), or via characteristics of the amplification curves. In the absence of the target, no fluorescent signal is generated. Created with BioRender (https://BioRender.com/h67z677).

quantify the pathogen concentration, which impedes applications such as monitoring of fungal or resistance loads.

A persistent difficulty with CRISPR-based diagnostics is reliably detecting mutations, such as single-nucleotide polymorphisms (SNPs), which are frequently associated with antimicrobial resistance. Under certain conditions, Cas12a can detect SNPs with high sensitivity and specificity[15]. However, Cas12a can also tolerate mismatches between its guide RNA (gRNA) and target nucleic acids, with these mismatches altering the kinetics of both *cis* and *trans* cleavage of Cas12–gRNA–target complexes[17–20]. These differences in reaction kinetics can be used to enable SNP detection using amplification-free tube-scale CRISPR reactions, but they have only achieved nanomolar limits of detection (LOD)[21].

Single-template methods have been used to enable highly sensitive pathogen quantification. In these methods, the initial sample is serially diluted to confine individual target molecules to picolitre reaction volumes, resulting in the binary presence or absence of the template in each compartment. The 'digital' signal obtained by counting the total number of target molecules allows accurate calculation of the number of molecules in the initial sample. Real-time digital diagnostics systems with kinetic monitoring, where the fluorescence within a compartment is followed as a function of time, have been shown to be useful for multiplexing of PCR reactions, when coupled with melting temperature analysis and machine learning algorithms[22–25], and for phenotypic-molecular antibiotic susceptibility testing with loop-mediated isothermal amplification (LAMP)[26,27].

Recent advances have applied digital CRISPR-Cas systems to quantitatively detect single templates. Digital CRISPR diagnostics have been implemented either without amplification[28–32] or as 'one-step' reactions, in which reagents are distributed into individual compartments and isothermal amplification occurs simultaneously with CRISPR cleavage and signal detection[33–35]. Typically, these digital systems rely on endpoint fluorescence measurements, with the observed signal being a convolution of both the isothermal amplification by recombinase polymerase amplification (RPA) and the Cas-based collateral cleavage of the reporter. Multiplexing in these digital CRISPR systems has been limited. The use of real-time kinetic measurements in CRISPR-based digital systems could enable improvements in sensitivity and specificity, and open the door to multiplexing that is not currently possible in tube-scale measurements or with classic digital CRISPR techniques.

In this study, we demonstrate an approach to CRISPR-based *C. auris* diagnostics with high sensitivity for all four major clades of *C. auris* and high specificity when challenged with simulated clinical samples, real clinical surveillance swabs and a potentially interfering panel of common fungi (Fig. 1). We develop a digital CRISPR diagnostic assay platform for the quantification of *C. auris* fungal load and demonstrate the use of single-template reaction kinetics with machine learning to harness Cas12a's target promiscuity for the simultaneous quantification of resistant and wild-type (WT) SNP subpopulations of the clinically relevant *FSK1* gene, which would be misdiagnosed as completely susceptible or resistant under standard reaction conditions.

Results

Sensitive and specific CRISPR-based detection of *C. auris*

We developed a highly sensitive CRISPR-based assay for the detection of *C. auris* from patient and environmental surveillance swabs based on the specific detection of the internal transcribed spacer (ITS) region of its genome. ITS is a common target sequence for fungal diagnostic development and has shown high specificity in PCR-based clinical *C. auris* assays[36,37]. We independently identified species-specific *C. auris* ITS regions using established bioinformatics techniques[38].

We first determined the analytical sensitivity and specificity of a bulk *C. auris* assay in standard reaction volumes with separate RPA amplification and CRISPR detection steps (two-step) using a combination of synthetic ITS2 DNA and DNA isolated from fungal cultures (Fig. 2a,b). After extensive optimization of RPA primers and gRNA (Supplementary Fig. 2 and Table 2), our assay successfully detected ≥25 aM of synthetic DNA target (Fig. 2a). Assay specificity was tested using DNA extracted from pure cultures of the four major geographical clades of *C. auris* compared with a clinically relevant fungal panel including several closely related yeasts (Fig. 2b). The assay successfully detected all *C. auris* clades while showing minimal background signal from other *Candida* and closely related yeasts (Fig. 2b). Results from a more extensive yeast panel confirmed the high specificity of the assay for *C. auris* (Supplementary Table 3), which is particularly important given the frequent misidentification experienced with current clinical diagnostic tests[5].

When clinical *C. auris* infection is suspected, current CDC guidelines recommend the use of surveillance culture collection via an axilla and groin skin swab, which are typically placed in Amies transport medium (composition in Supplementary Table 5)[39]. To demonstrate clinical utility and assess the potential inhibitory effects of Amies transport medium, we tested our two-step assay using a single-blind panel of clinically relevant simulated swab samples that were created from pure *C. auris* cultures resuspended at a range of relevant colony-forming

https://doi.org/10.1038/s41551-025-01597-0

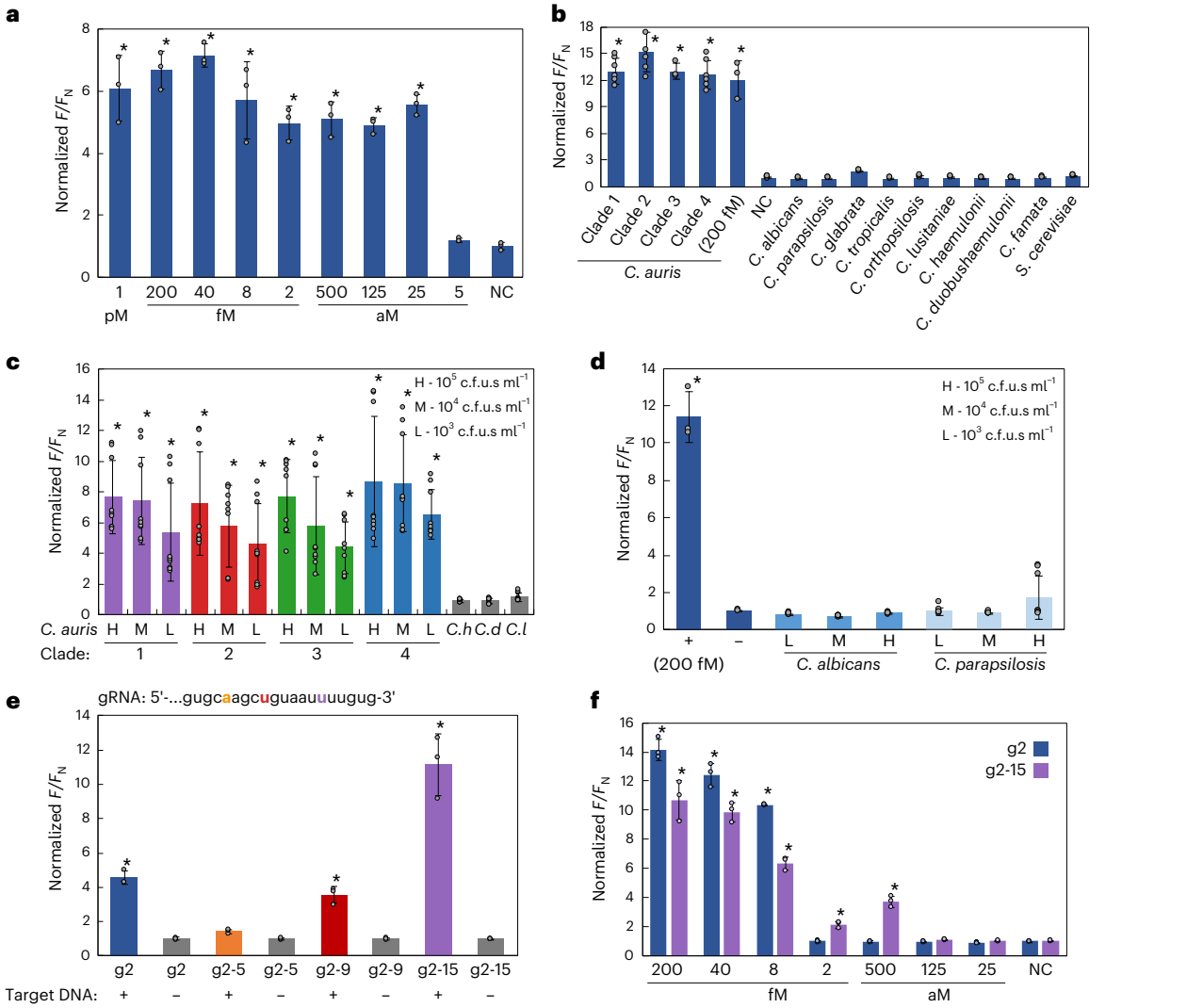


Fig. 2 | SHERLOCK enables specific and sensitive detection of *C. auris*. **a**, Two-step measurements with decreasing concentrations of synthetic ITS2 target DNA establish the two-step limit of detection (LOD) in the low aM range. **b**, Two-step measurements of genomic DNA extracted from cultured cells of four major clades of *C. auris* and several related species were tested at sample concentrations of 1 ng µl^{-1}. Two isolates were available for testing our ability to detect Clades 1, 2 and 4 of *C. auris*; in these cases, the results are the mean of the two samples, each measured as technical triplicates ($n = 6$). **c**, Two-step measurements showing detection of *C. auris* from all four major clades in simulated swab samples at different concentrations of colony-forming units (high (H): 10^5 c.f.u.s ml^{-1}, medium (M): 10^4 c.f.u.s ml^{-1}, low (L): 10^3 c.f.u.s ml^{-1}). No non-specific signal is demonstrated in samples of *C. haemulonii* (*C.h*), *C. duobushaemulonii* (*C. d*) and *C. lusitaniae* (*C. l*). Results are the mean of technical triplicates each day, repeated on 3 different days ($n = 9$) using two different instruments to demonstrate robustness. **d**, Two-step measurements of samples with *C. albicans* and *C. parapsilosis* at high (H), medium (M) and low (L) concentrations (c.f.u.s ml^{-1} as in Fig. 1c). Three *C. albicans* and *C. parapsilosis* samples were tested at each concentration, each as a technical triplicate ($n = 9$). **e**, One-step performance of the *C. auris* SHERLOCK assay with a gRNA perfectly matching the ITS sequence (g2-blue) or with one engineered mismatch in the gRNA. The mismatch was engineered at different distances from the Cas12a protospacer adjacent motif (PAM) site, which occurs at the 5′ end of the complementary sequence of gRNA shown (g2-5 (orange), 5 bp from PAM; g2-9 (red), 9 bp from PAM; g2-15 (purple), 15 bp from PAM). **f**, One-step performance of the *C. auris* SHERLOCK assay with a gRNA perfectly matching the ITS2 sequence (g2, blue) and with one engineered mismatch in the gRNA 15 bp from the Cas12a PAM (g2-15, purple), demonstrating the increase in one-step sensitivity through addition of a deliberate gRNA mismatch. For results in **a**–**f**: data are shown after 90 min; fluorescence signal (F) is normalized to the mean of the negative control (F_N); using a threshold of $F/F_N > 2$, positive signals marked with an *; PC, positive control (10 fM synthetic *C. auris* ITS DNA); NC, negative control (water instead of target DNA); unless otherwise specified, data are presented as the mean ± s.d. of technical triplicates ($n = 3$).

units (c.f.u.s ml^{-1}) in Amies medium (Fig. 2c). Since Amies medium is the standard transport medium used for clinical *C. auris* samples, this is the only sample matrix we expect to encounter in practice. All samples were prepared at the Wadsworth Center of the New York State Department of Health to represent clinical samples after fungal collection and heat inactivation. All four *C. auris* clades were positively identified from these samples across all concentrations tested, with no false positive signals from three closely related species: *C. haemulonii*, *C. duobushaemulonii* or *C. lusitaniae*.

Next, we evaluated the performance of the assay on simulated swab samples of *Candida albicans* and *Candida parapsilosis* (Fig. 2d). These two pathogens are observed with the highest frequency in patient surveillance samples and environmental surveillance swabs[40]. Neither *C. albicans* nor *C. parapsilosis* generated false positive signals at any of the concentrations tested. The above experiments demonstrate that our *C. auris* ITS2 assay reliably distinguishes *C. auris* from other species, including closely related yeasts, with high specificity and is fully compatible with swabs collected according to current clinical practice.

After establishing the analytical sensitivity and specificity of our assay design, we sought to streamline the protocol by combining the amplification and Cas12a detection into a one-step format. This format shortens the sample time-to-result and enables quantification of fungal load using digital microfluidics. The LOD of the one-step assay is frequently worse than with the two-step format[41], so we screened the one-step assay using both the optimal gRNA selected for the two-step format as well as gRNA with intentional single-nucleotide mismatches at strategic distances from the protospacer adjacent motif (PAM) of the Cas12a enzyme (Fig. 2e). We achieved a notable increase in signal in the one-step assay using a gRNA with a mismatch introduced in the PAM-distal region (15 bp), whereas mismatches in the PAM-proximal region decreased assay signal. We then compared the analytical sensitivity of the one-step assays with both the perfectly matched gRNA and the gRNA with the intentional mismatch 15 bp from the PAM (Fig. 2f). The lowest detectable concentration of the one-step assay using the perfectly matched gRNA was ~320× worse (~8 fM) than with the two-step configuration (~25 aM). However, using the mismatched gRNA in the one-step assay substantially improved the lowest detectable concentration (~500 aM). Literature studies indicate that Cas is tolerant to PAM distal mismatches, with mismatches impacting both the *cis* and *trans* cleavage kinetics[17–20]. These changes in kinetics are discussed further in the context of single-nucleotide mutation detection in the sections that follow.

Optimization of real-time dSHERLOCK for absolute quantification

To address the need for a method that enables the quantification of fungal loads in surveillance swab samples[6], we developed a single-template version of the SHERLOCK assay called digital SHERLOCK (dSHERLOCK) that uses the binary (presence or absence) nature of each template in a partition when the sample is sufficiently dilute. We used commercially available QuantStudio 3D Digital PCR 20 K v.2 Chip microarrays from Applied Biosystems, which have previously been used for LAMP assays[26,42]. The arrays have a 1 cm^2 reaction plate with 20,000 individual partitions comprising a volume of ~750 picolitres each. The total reaction volume loaded onto a microarray is 14.5 microlitres. Compartmentalization occurs via capillarity using a plastic loading 'blade'. The reaction mixture was loaded, the solution remaining on the surface was briefly evaporated, and an immiscible fluorocarbon oil was applied to isolate the compartments into individual reaction volumes.

We developed a computational pipeline to obtain real-time reaction kinetics from dSHERLOCK reactions in individual partitions. We identified partitions and generated image segmentation masks using the reference dye ROX (Fig. 3a), which enabled tracking of compartments in a fluorescence channel independent of our reporter dye. We occasionally observed interconnected compartments, as well as suboptimal wetting of the microarray. Several buffer conditions were screened and we found that addition of 0.1% Polysorbate 20 ameliorated these problems (Supplementary Fig. 3). On average, we observed 18,000 compartments per microarray.

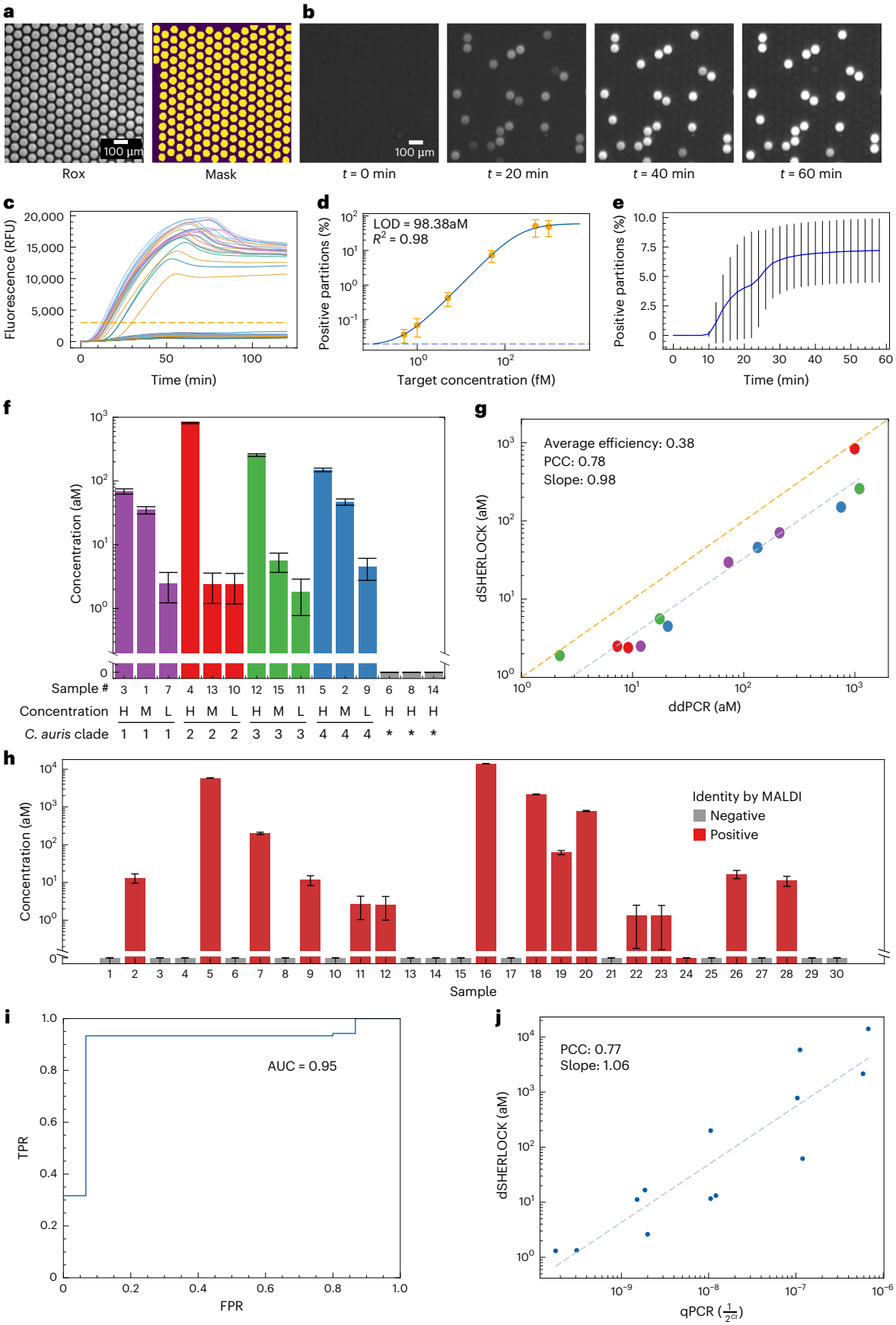
We quantified the fluorescence intensity of dSHERLOCK reactions over time and extracted the reaction kinetics within individual partitions using the previously generated masks and correcting for small movements between timepoints. Increasing signals were observed in compartments containing a target DNA molecule recognized by the Cas as early as 20 min after initiation of heating to 37 °C (Fig. 3b). An empirically chosen threshold was drawn to separate partitions with active reactions from those that were not active (Fig. 3c). On the basis of triplicate measurements at the mid-range digital concentration of 50 fM, we determined that a fluorescence intensity threshold of ~3,000 relative fluorescence units (RFU) corresponded to the maximum fluorescence of the negative compartments (Supplementary Fig. 4). Target DNA concentrations were calculated using Poisson statistics from the aggregate number of partitions with fluorescence intensity greater than the threshold.

We next asked whether real-time digital SHERLOCK could accurately quantify DNA from *C. auris*, using our optimized one-step assay (Fig. 2f). A calibration curve using the dSHERLOCK system for the detection of *C. auris* was recorded by loading microarrays with a range of synthetic *C. auris* target DNA concentrations (Fig. 3d). A 4-parameter logistic curve was fit to the signal-generated concentrations and the LOD was calculated to be 100 aM or 300 copies in the sample (see detailed discussion in Supplementary Information). The linear regime of quantification was found to be ~1–100 fM (see Supplementary Information 1). We also verified the ability of real-time dSHERLOCK to quantify *C. auris* in simulated swab samples and found that Amies medium and non-specific DNA had negligible effects (Supplementary Table 4 and Fig. 5). Similarly, we assessed the impact of pre-compartmentalization reaction time on absolute quantification by testing durations ranging from 60 to 180 s. The measured value was found to be independent of the time before compartmentalization in this range with $p = 0.32$ as obtained by weighted linear regression, indicating that the dSHERLOCK reaction is robust to fluctuation in reaction initiation times (Supplementary Fig. 6). For practical purposes, we selected a 1-min pre-compartmentalization time before loading the chips to efficiently achieve all reaction steps (that is, pipetting, mixing, loading and compartmentalization), which could rarely be completed in less than 45 s.

We wished to determine the optimal reaction time for a dSHERLOCK experiment. We found that real-time dSHERLOCK enables a simple evaluation of every timepoint as a potential endpoint (Fig. 3e). Detection of *C. auris* occurred as early as 10 min and reliably 20 min after the measurement had started, when partitions could be statistically

Fig. 3 | dSHERLOCK accurately quantifies *C. auris* in simulated and clinical swab samples. **a**–**c**, dSHERLOCK tracks the fluorescence of individual partitions over time by the concurrent recording of fluorescence micrographs of (**a**) a reference dye channel from which a mask is generated that represents the positions of microwells and (**b**) a reporter dye channel, in which an increase in fluorescence intensity over time is observed in partitions that amplify and detect a dsDNA target molecule. Applying the positional mask to the reporter dye channel enables the extraction of (**c**) plots of fluorescence intensity over time for representative individual partitions (coloured lines). A fluorescence intensity threshold (orange dashed line) can be employed to separate amplified partitions from non-amplified partitions. **d**, Plot of signal output (% of positive partitions) as a function of concentration recorded in triplicate after 2.5 h of measurements with synthetic *C. auris* ITS2 DNA. Error bars represent standard deviation of 3 distinct replicates. Background was calculated as the mean of 3 distinct samples without DNA plus 3× their standard deviation. The calibration curve was fit using a 4-parameter logistic regression, minimizing the sum of square errors, to yield an R^2 value of 0.98. The LOD (98.4 aM) was calculated as the point where the fit curve intersects the background. **e**, Percentage positive partitions over time, using 3,000-RFU threshold. Error bars indicate 95% confidence intervals (CIs) ($n = 3$ independent replicates, 50 fM [target]). **f**, dSHERLOCK quantification of *C. auris* clades 1–4 in simulated swab samples (high (H): 10^5 c.f.u.s ml^{-1}, medium (M): 10^4 c.f.u.s ml^{-1}, low (L): 10^3 c.f.u.s ml^{-1}; corresponding to 500, 50 and 5 c.f.u.s per sample, respectively) and *C. haemulonii, C. duobushaemulonii, C. lusitaniae* at 10^5 c.f.u.s ml^{-1} (*). Error bars indicate Poisson noise ($n = 15$ samples). **g**, ddPCR vs dSHERLOCK absolute quantification of *C. auris*. Curves fit as linear functions minimizing squared error. Efficiency = [dSHERLOCK]/[ddPCR] averaged over all samples. **h**, Blinded dSHERLOCK quantification of *C auris* from $n = 30$ clinical residual composite surveillance swabs. Samples were identified as positive (red) or negative (grey) for *C. auris* by MALDI. Error bars indicate Poisson noise. **i**, Receiver operating characteristic (ROC) curve plots false positive rate (FPR) versus true positive rate (TPR) for detection of *C. auris* in clinical surveillance swabs varying fluorescence intensity threshold with an area under the curve (AUC) of 0.95. **j**, Correlation between quantification by dSHERLOCK and qPCR. Pearson correlation coefficient (PCC) was 0.77, indicating a strong positive correlation when excluding outliers as determined by studentized residuals analysis (Supplementary Table 8 and Fig. 9).

https://doi.org/10.1038/s41551-025-01597-0



distinguished from background. Absolute quantification of the fungal load in the sample was achieved after only 40 min, when no additional partitions turned positive.

Next, the performance of dSHERLOCK was tested using the single-blind simulated swab panel, as described previously (Fig. 2c). Sample unblinding occurred only after dSHERLOCK assay results were obtained and reported. The concentrations measured by dSHERLOCK agreed well with pre-assay c.f.u.s across all four clades and concentrations (Fig. 3f). Quantitative information was obtained from all four *C. auris* clades and the assay did not detect the samples of related *Candida* species, indicating high specificity.

We next evaluated the quantification of dSHERLOCK compared to digital droplet PCR (ddPCR) (Fig. 3g). In general, ddPCR and dSHERLOCK showed close agreement in relative concentration between samples but differed in absolute c.f.u.s (detailed discussion in Supplementary Information). The probability of detection ('efficiency') with dSHERLOCK was 38% relative to ddPCR, similar to other quantitative isothermal methods[42]. This difference can be ascribed to the fact that Cas12a *cis* cleavage destroys the target molecule, potentially occurring before amplification[43]. We observed this effect to be highly reproducible and thus, a simple correction constant could be applied on the basis of the linearity and overlapping ranges of both methods. A comparison between dSHERLOCK and ddPCR revealed a high degree of consistency in amplification efficiency across all four *C. auris* clades, as reflected by the slope of 0.98 in the log–log plot (Fig. 3g). This suggests that despite slight variations, the overall performance of dSHERLOCK remains reliable for quantification across different clades, with the minor correction factor applied ensuring accurate alignment between the two methods. Both ddPCR and dSHERLOCK showed reduced calculated c.f.u.s relative to prepared c.f.u. counts (Supplementary Fig. 7), but this may be due to target degradation during shipment and storage because the samples were prepared and blinded at one institution, and shipped and stored at another institution.

To further evaluate the clinical applicability of dSHERLOCK to detect *C auris*, we challenged the platform with a blinded panel of 30 naris–axilla–groin swabs collected as surveillance samples directly from patients. Samples were heat killed but an explicit lysis step was omitted. After measurement using dSHERLOCK, the panel was unblinded with results compared to MALDI mass spectrometry and qPCR. Using the optimal reaction time of 40 min, determined in Fig. 3e, dSHERLOCK correctly identified 14/15 positive samples and 15/15 negative samples, resulting in an accuracy of 96.7% (Fig. 3h). The performance of dSHERLOCK as a tool for the detection of *C. auris* is further illustrated by an area under the curve (AUC) of 0.95 in a receiver operating characteristic (ROC) curve drawn by varying the fluorescence intensity threshold for classifying a well as positive from high to low (Fig. 3i). Detection performance was robust to the specific choice of fluorescence threshold, with all metrics retaining their maximum value in a range from 2,500 to 4,000 RFU (Supplementary Fig. 8).

To examine the accuracy of fungal load quantification in clinical samples, we compared concentrations measured by dSHERLOCK with measurements obtained by qPCR (Fig. 3j). The analysis showed a moderate correlation between the two quantities with a Pearson correlation coefficient (PCC) of 0.4, demonstrating that dSHERLOCK is able to quantify fungal load in clinical swab samples collected directly from patients. This correlation is notably lower than the PCC of 0.78 between dSHERLOCK and PCR observed in synthetic swab samples (Fig. 3g), which exhibited a strong positive correlation. The lower correlation in patient samples is influenced by a single outlier (Patient 11, PCR cycle threshold (C_t) = 19.8, Supplementary Fig. 9), which had a high fungal load by qPCR, but low signal by dSHERLOCK. We identified this point as an outlier on the basis of its studentized residual, which is 4.92 standard deviations from the expected value derived from the linear fit. Excluding this sample increases the PCC between dSHERLOCK and PCR in clinical samples to a strong correlation of 0.77 (Fig. 3j), in agreement with the synthetic swabs and supporting the utility of dSHERLOCK for quantification across a clinically relevant range of pathogen concentrations.

The single clinical false negative result (Patient 24; C_t = 32.5) falls below the dSHERLOCK platform's practical LOD. On the basis of the regression between the clinical sample C_t values and dSHERLOCK measurements, we find that the practical LOD of the system is comparable to that of qPCR (Supplementary Fig. 9). For comparison, *C. auris* was successfully detected in other clinical samples with similar C_t values (C_t = 31.6 and 32.4). Notably, C_t values above 32 are generally considered very low pathogen burden in surveillance samples (<10 c.f.u.s ml^{-1}), and both platforms begin to approach their detection limits in this range. These results indicate that dSHERLOCK exhibits practical analytical sensitivity limitations comparable to those of qPCR, and detecting low-burden infections remains a challenge across both platforms.

Quantification of echinocandin resistance using dSHERLOCK

Up to 90% of all *C. auris* isolates show resistance to the antifungal fluconazole[4]. Thus, echinocandin antifungals are the current preferred treatment option and generally remain effective, although resistance has increased substantially[4]. We designed a dSHERLOCK assay for echinocandin resistance on the basis of detection of a pathogenic SNP in the *FKS1* gene, *FKS1* S639F, which results from a C1916T transition[44]. Using a gRNA that was perfectly complementary to the mutant allele resulted in detectable signal from the mutant allele and unexpectedly high signal from the detection of the wild-type allele, despite the single base pair mismatch between the gRNA and WT allele at the site of the SNP (Fig. 4a). Introducing a mismatch in the gRNA two nucleotides from the SNP of interest, in the PAM distal direction from the SNP, resulted in improved specificity and sensitivity for the mutant allele (Fig. 4b). This gRNA has a single intentional mismatch as compared to the mutant allele sequence, but has two mismatches compared to the wild-type allele (mismatch and SNP), which knocks out tube-scale signal from the wild-type allele (Fig. 4b). This strategy has previously been described to aid in SNP-detecting guide design[41]. We observed a similar effect in our design of a dSHERLOCK one-step assay for an SNP mutation in the *ERG11* gene conferring resistance to azole antifungals (Supplementary Fig. 10).

Given the higher signal with single mismatch gRNA compared with gRNA perfectly complementary to the MT allele, we sought to determine whether the difference in final fluorescence intensity between the mutant and wild-type templates was due to a difference in the absolute number of templates detected or a result of distinct reaction kinetics. We performed dSHERLOCK *FKS1* assays in triplicate at 50fM and quantified the results using a threshold of 3,000 RFU after 2.5 h (Fig. 4c). Surprisingly, we observed that both the mutant *FKS1* allele, with one mismatch to the gRNA, and the wild-type allele, with two mismatches to the gRNA, had an equal percentage of partitions amplified, indicating an equal number of templates detected (see Supplementary Fig. 4 for choice of fluorescence threshold). Thus, the difference in fluorescent signal between reactions with the mutant and the wild-type alleles observed in the tube-scale reaction (Fig. 4ab) is not due to the specificity of gRNA to hybridize and detect the wild-type target molecule (that is, a difference in the number of molecules detected), but is related to the unique kinetics of detecting each template (that is, template amplification, the efficiency of template recognition, or the subsequent *trans* cleavage of fluorescent reporter molecules).

We next asked whether quantification of the two alleles could be resolved temporally by comparing when a reaction reaches a fluorescence intensity threshold, which we defined as time to positivity (TTP, Fig. 4d). To ensure specificity against potentially amplifiable, non-target DNA (for example, from skin cells or environmental contaminants), 50 fM of both scrambled synthetic DNA sequence of the same length and a pure water sample were used as controls. We observed that detection of the mutant allele occurred with faster reaction kinetics

https://doi.org/10.1038/s41551-025-01597-0

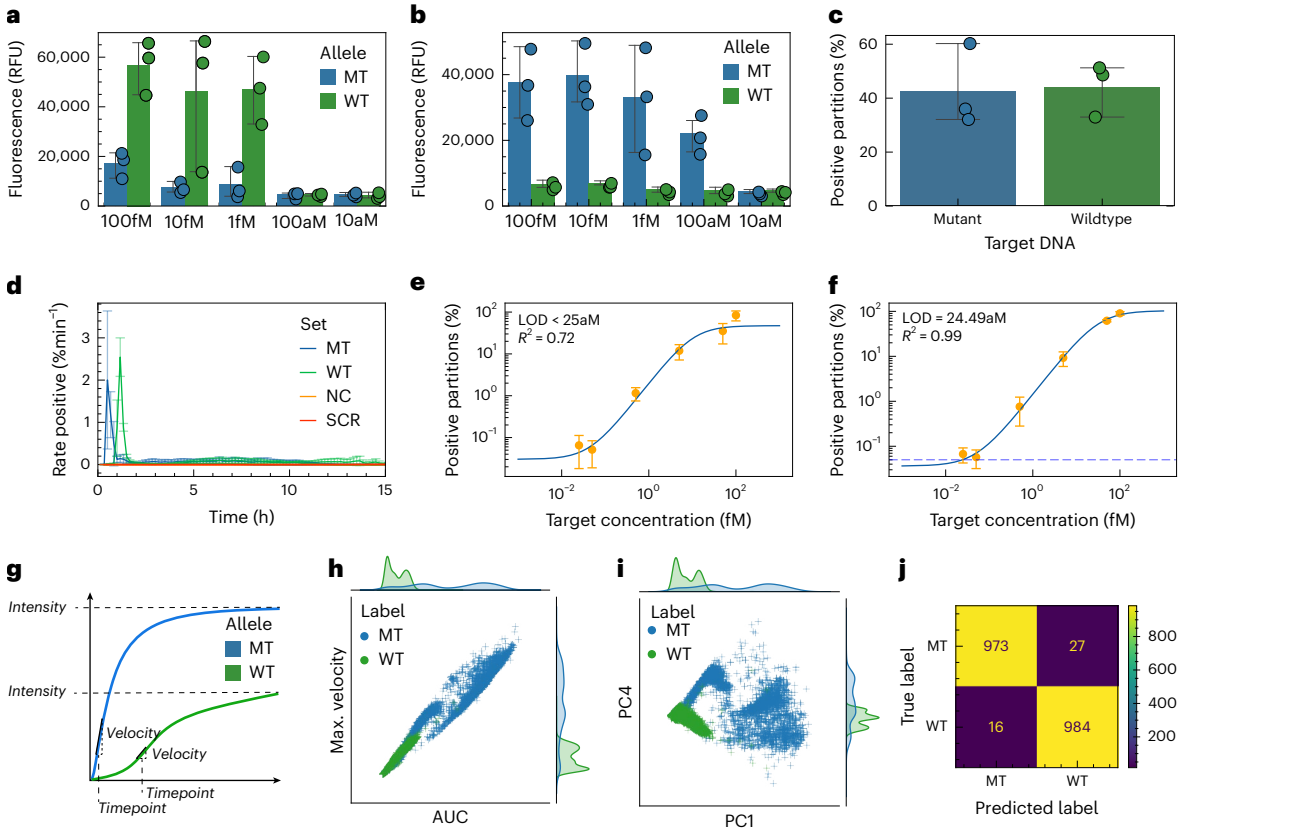


Fig. 4 | SNPs of the *FKS1* resistance gene exhibit distinct kinetics in dSHERLOCK. Plot of fluorescence after 2.5 h as a function of concentration for standard-scale one-step dSHERLOCK assays for detecting an SNP in the *FKS1* gene with (**a**) a gRNA perfectly complementary to the *FKS1* mutant allele and (**b**) a gRNA that is complementary to the *FKS1* mutant allele except for one intentionally added mismatch. The added mismatch is two nucleotides from the SNP of interest, in the PAM distal direction. Data indicate mean ± 95% CI ($n = 3$ technical replicates). **c**, Bar plot of percent positive partitions using dSHERLOCK to detect synthetic DNA of mutant and the wild-type allele at 50 fM sample concentration after 2.5 h with a threshold of 3,000 RFU. Data indicate mean ± 95% CI ($n = 3$ technical replicates). **d**, Line plot of the percent compartments that cross the positive fluorescence threshold as a function of time. Scrambled (SCR) represents a synthetic DNA of a scrambled sequence, equal in length to synthetic DNA targets of both mutant and wild type, measured at a sample concentration of 50 fM. No DNA control (NC) represents samples of pure nuclease-free water. Intervals between images were 10 min and all reactions were prepared as 3 distinct samples ($n = 3$). Data represent mean ± s.d. **e**,**f**, Plot of dSHERLOCK *FKS1* calibration curves using a 3,000-RFU threshold for (**e**) mutant allele, evaluated after 1 h and (**f**) wild-type allele after 2 h. Data represent mean ± s.d. of distinct triplicate measurements. **g**, Schematic amplification trajectories of individual partitions (RFU over time) showing extractable features such as intensity, velocity, AUC and timepoints to quantify curve shape. Extracted features can be found in Supplementary Table 6. **h**, Scatterplot with kernel densities of continuous features in training data, such as maximum velocity and AUC, shows a high degree of correlation. Labels correspond to ground truth. **i**, Scatterplot with kernel densities of principal components 1 vs 4 in training data illustrates separation between mutant and wild type with low correlation. Components 1 and 4 were chosen for illustration purposes only to show maximum visual separation of mutant and wild type in an orthogonal 2D space. Labels correspond to ground truth. **j**, Confusion matrix from a random-forest classifier on holdout test dataset of $n = 1{,}000$ reactions of each allele. Features for classification were calculated after 2 h of measurements. Colour bar indicates reaction counts (n).

than detection of the wild-type allele, while neither scrambled DNA nor water controls resulted in signal amplification.

Individual reaction compartments containing either mutant or wild-type target alleles showed distinct reaction kinetics but comparable endpoint fluorescence (Supplementary Fig. 11). However, while the reaction kinetics between the two alleles are reliably different in a given chip, the degree of the difference varies between chips within a group and between experimental groups. Batch effects cause positive partitions to reach varying fluorescence intensities and exhibit different reaction kinetics, which impedes allele separation using simple thresholds. No single threshold that was valid between all batches could be found to accurately separate mutant and wild type (Supplementary Fig. 12). On the basis of the observed difference in kinetics between alleles, we recorded calibration curves after 1 h and 2 h for the mutant (Fig. 4e) and wild-type (Fig. 4f) target DNA alleles, respectively, corresponding to the timepoints when no additional partitions turned positive. We found the assay to perform equally well at quantifying the mutant and wild type (see detailed discussion in Supplementary Information).

Classification based on multiple reaction kinetics features enhances allele discrimination

Due to complications arising from batch effects, which prevent the use of simple reaction thresholds or TTP to separate target alleles, we extracted additional reaction kinetics features from each compartment (Supplementary Table 6). Features were categorized as either continuous variables, such as intensities and velocities, defined as the change in intensity between two measurements, or the timepoints when certain reaction characteristics were observed (for example, maximum intensity or maximum velocity) (Fig. 4g). Many continuous features were highly correlated and scaled (Fig. 4h). Orthogonal features were obtained using principal component analysis (PCA). All eight principal components (PCs) were retained for classification, providing the classifier with less correlated variables, some of which presented good separation between mutant and wild type (Fig. 4i).

To reduce the classification task to a binary choice between mutant and wild type, we developed an algorithm to remove non-amplifying compartments on the basis of their maximum fluorescence intensity.

https://doi.org/10.1038/s41551-025-01597-0

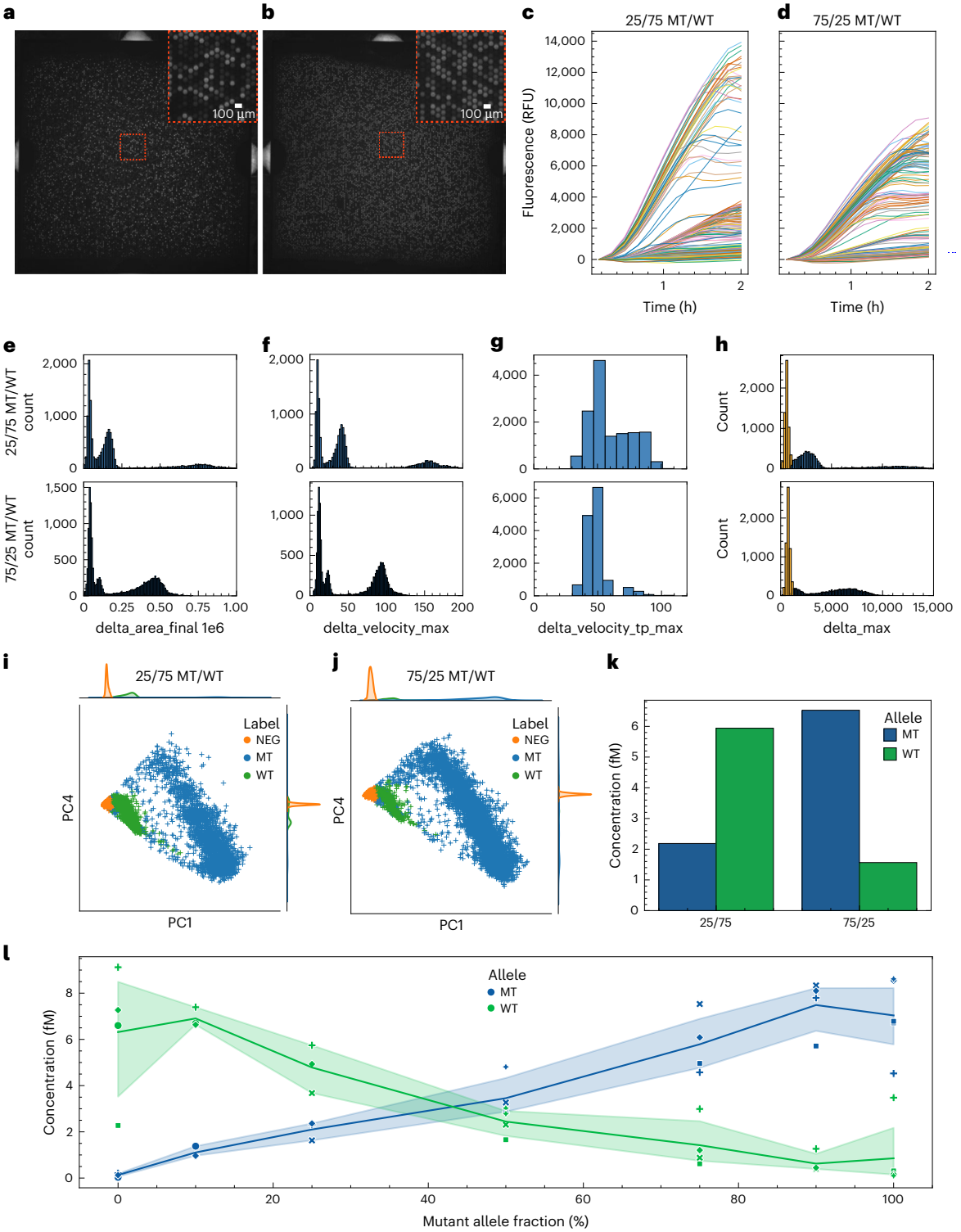


Fig. 5 | dSHERLOCK simultaneously and rapidly quantifies SNP alleles in heterogeneous samples. a,**b**, Fluorescence micrographs of reporter dye channel after 2 h, with magnification for emphasis, of microarrays containing synthetic DNA at a total concentration of 50 fM with allele fractions of (**a**) 25% mutant and 75% wild type and (**b**) 75% mutant and 25% wild type. Representative examples of 3 and 4 independent replicates, respectively. **c**,**d**, Plots of fluorescence over time for microarrays shown in **a** and **b**. Intervals between images were 10 min. **e**–**g**, Histogram plots of partitions with respect to representative features extracted from trajectories shown in **c** and **d**. Visualized features are (**e**) AUC, (**f**) maximum velocity and (**g**) timepoint of maximum velocity. **h**, Negative partitions (orange-black) as labelled by GRANITE on the maximum fluorescence intensity and positive partitions (blue). **i**,**j**, Scatterplots of partitions in principal components 1 and 4, chosen for illustration only on the basis of good visual separation of groups. Labels for mutant (MT) and wild type (WT) were determined by random-forest classification for illustrative purposes. **k**, Bar plot of concentrations of each allele in both chips as determined by random-forest classification and Poisson statistics. **l**, Plot of concentrations of each allele, as determined by the classification scheme, from chips containing 0%, 10%, 25%, 50%, 75%, 90% or 100% of mutant allele at a constant total sample DNA concentration of 50 fM. For each mutant allele fraction, chips were prepared at least in triplicates across separate batches on different days. Lines represent means and shaded areas represent 95% CIs. Marker shapes represent batches. $n = 54$ chips across 6 independent batches.

These negative compartments followed a Gaussian distribution leading us to employ a customized Gaussian fitting algorithm termed GRANITE (Gaussian robust algorithm for negative identification via thorough estimation) (Supplementary Fig. 13).

A random-forest classifier was built on 15,000 randomly selected trajectories and tested on a holdout set of 1,000 trajectories from each class to estimate performance (Fig. 4j). The classifier correctly identified 97.3% of mutant alleles and 98.4% of wild-type alleles, for a classification sensitivity of 98.3%, classification specificity of 97.3% and classification accuracy of 98%.

Simultaneous quantification of multiple alleles in heterogeneous mixtures

With the development of a dSHERLOCK classification scheme for homogeneous populations, we wished to determine whether this technique could be applied to multiplexed detection within heterogeneous populations. This could be useful for monitoring the development of resistant subpopulations. We evaluated whether dSHERLOCK could simultaneously quantify *FKS1* mutant and wild-type alleles using mixed targets at a total DNA concentration of 50 fM, maximizing the number of partitions loaded with a single template. We recorded images every 10 min for 2 h and subsequently applied all previously described data-processing steps to obtain a concentration measurement for both alleles via the difference in kinetics between the reactions. After 2 h, a difference in fluorescence intensities was clearly visible between compartments loaded with mutant target DNA and those with wild-type target DNA (Fig. 5a,b). However, manual classification for each compartment was not a trivial task. Endpoint fluorescence intensity allowed separation of wild-type and mutant *FKS1* target for many compartments, but a substantial population of compartments had intensities that fell between allele groups. Batch effects also resulted in chip-to-chip heterogeneity (Fig. 5c,d), validating the importance of GRANITE processing in the classification scheme (Supplementary Fig. 10).

For the continuous reaction kinetics features, both alleles followed approximately Gaussian or tailed Gaussian distributions (Fig. 5e,f), while the discrete timepoint features did not follow clearly recognizable distributions (Fig. 5g). Maximum intensity plus GRANITE were used to identify negative compartments and to exclude them from the validation dataset (Fig. 5h). Applying the previously calculated principal component decomposition, we observed a clear separation in some PCs (Fig. 5i,j). Subsequent classification then labelled the remaining compartments as mutant or wild type, which enabled us to calculate sample concentrations of each allele in each chip via the Poisson distribution (Fig. 5k).

To evaluate whether dSHERLOCK could be used to predict both the identity and concentration of each allele in a mixed population, the mutant allele was titrated as 0%, 10%, 25%, 50%, 75%, 90% and 100% relative to the wild-type allele in batches of between 2 and 6 chips for each allele fraction (Fig. 5l). dSHERLOCK accurately and reliably quantified the allele fraction in multiple independent batches. Although the efficiency of the dSHERLOCK *FKS1* assay caused the measured sample concentration to be approximately six times lower than expected, the good linearity and precision between batches showed that one could apply a constant factor to recover the absolute sample target concentration for each allele simultaneously from a single 2-h measurement. We hypothesize that this low efficiency arises from the competition between template amplification and template cleavage. Thus, splitting SHERLOCK reactions into single-template partitions enables us to obtain reaction kinetics for individual target molecules. On the basis of these kinetics, we are able to distinguish and separately quantify different target molecules in a sample. Through this method, dSHERLOCK detects the allelic fraction of a resistant strain in a mixed sample, which would not be discernible under standard SHERLOCK reaction conditions.

Discussion

In this work, we describe dSHERLOCK, a single-molecule nucleic acid platform for the quantification of double-stranded DNA (dsDNA) targets using CRISPR/Cas and isothermal amplification. The platform was applied to the quantification of the emerging fungal pathogen *C. auris* in both contrived and real clinical surveillance swab samples at clinically relevant concentrations in an appropriate sample-collection matrix. Machine learning was applied to features extracted from single-template reaction kinetics for the simultaneous quantification of SNP alleles conferring resistance of *C. auris* to antifungals. Single-template reactions revealed that tube-scale target specificity was the result of distinct reaction kinetics for a template, rather than the absolute number of target molecules detected. These assays show the usefulness of one-step reaction kinetics, CRISPR diagnostic kinetics in a single-template system and a multiplexed CRISPR diagnostic assay using a single guide.

dSHERLOCK reliably detected the presence of *C. auris* in both simulated and clinical swab samples at clinically relevant concentrations after just 20 min and enabled absolute quantification after 40 min. Since dSHERLOCK was shown to measure the target DNA in the relevant sample transport medium directly, no dedicated nucleic acid extraction step was necessary. We hypothesize that the time scales and minimal sample preparation requirements of these assays could enable swift decision-making in a clinical setting, with quantitative tracking resulting in the ability to contain outbreaks in healthcare facilities. In the clinic, we envision that, under ideal conditions, our assay would first provide presence/absence information within the first 20 min, followed by quantification after 40 min. Similar to standard antibiotic susceptibility testing (AST), dSHERLOCK-based genetic resistance testing would be conducted as a follow-on experiment. Further clinical validation will be necessary to establish the explicit relationship between genotypic and phenotypic AST, ensuring the assay's utility in real-world settings. At present, clinical guidelines do not define actionable thresholds for low-frequency resistance mutations in individual swabs being tested for *C. auris*[45–47]. Future work will be needed to determine whether mixed resistance genotypes within individual patients occur at clinically meaningful levels and to define allele fraction thresholds that would guide antifungal therapy.

As has been described in the literature, a competition exists between the isothermal amplification and the *cis* cleavage of the templates[43]. In our platform, this competition may occur before or immediately after compartmentalization, meaning that once a template is cleaved, it can no longer serve as a substrate for RPA and is effectively lost to the assay. This loss mechanism probably contributes to the lower observed detection efficiency for dSHERLOCK compared with ddPCR, which relies solely on amplification. Nonetheless, our platform offers insights into the kinetics of SHERLOCK reactions, and further study may enable more streamlined primer and guide selection, perhaps untangling the two reactions, to enable rational design. This approach stands in contrast to tube-scale experiments, which favour the fastest or most prevalent templates. Further optimization of reaction conditions, such as compartment size, enzyme selection and buffer composition could improve assay performance to enable direct single-molecule detection without nucleic acid amplification.

We expect that new applications could arise from the simultaneous quantitative and multiplexing capabilities described in this manuscript. We anticipate that dSHERLOCK could be useful for the quantification of emerging viral resistance, for example, testing for patients living with HIV to quantify both the viral load as well as the status of resistance mutations, or during viral and bacterial surveillance, as is now common in wastewater[48] and food production[49], to identify outbreaks early.

Methods

Identification of species-specific target sequences

Previously established bioinformatics techniques for the identification of species-specific nucleic acid sequences were used[38]. Suitable

target sequences were required to have >99% target specificity against other infectious agents and related species. All available high-quality *C. auris* genomes were analysed and compared to reference genomes for all other *Candida* related species, as well as broader non-redundant nucleotides in the NCBI database. The applied bioinformatic approach splits genomes into small 20–30 nucleotide *k*-mers. Then, using a series of efficient algorithms, genome-wide analyses were performed to identify regions that are specific to *C. auris*. In this case, the assay targets the ITS region of *C. auris*, which is in line with the gold standard qPCR assay[37]. Alignments of these areas show that our assay performs identically to the standard qPCR assay[37]. Both assays had perfect matches to all 49 strains, spanning all clades, that are available in NCBI (see Supplementary Table 7).

SHERLOCK RPA primer and gRNA screening

Conserved regions identified from the bioinformatics analysis were used to generate target RPA primers and gRNA sequences. RPA primers were purchased from Integrated DNA Technologies (IDT). The CRISPR gRNA was produced by in vitro transcription from synthetic DNA sequences purchased from IDT using the HiScribe T7 Quick High Yield RNA Synthesis kit (New England Biolabs, NEB) and purified using the RNA Clean and Concentrator kit (Zymo). A quenched fluorescent ssDNA reporter with a 5′ end-labelled FAM group and a 3′ end attached to an Iowa Black quencher (56-FAM/TTATT/3IABkFQ) was purchased from IDT. RPA primer screens were conducted using 10 µl reaction volumes of the RPA basic kit (TwistDx) spiked with unique primer sets to final concentrations as recommended in the manufacturer instructions: 14 mM magnesium acetate, 490 µM RPA primers each and 0.6× rehydration buffer incubated at 40 °C for 30 min. Initial screen gRNAs were constructed for expected RPA amplicons of different sequence targets. Collateral degradation of ssDNA reporter upon Cas12a activation was measured by mixing 2 µl of an RPA primer screen reaction into a 10 µl reaction volume with final concentrations of 100 nM Cas12a (NEB), 200 nM gRNA, 1× NEB 2.1 buffer and 1 µM ssDNA reporter. We incubated the mixture at 40 °C for 120 min and measured fluorescence kinetics in a BioTek Synergy NEO HTS plate reader (BioTek Instruments) with readings every 3 min (excitation: 485 nm; emission: 535 nm). The best-performing RPA primer sets from sequence targets were selected for further testing of two to three gRNAs constructed from the RPA amplicon region, using the same protocol.

Tube-scale two-step Sherlock

RPA reactions were prepared per TwistAmp Basic RPA pellet (TwistDx) and following manufacturer instructions by using 29.5 µl of RPA rehydration buffer (TwistDx) and 480 nM of each primer (IDT). Double-stranded target DNA and nuclease-free water were combined to add up to 47.5 µl. As a last step, 2.5 µl of 280 mM magnesium acetate was added. The reactions were incubated at 40 °C for 30 min. Cas reaction mixes were prepared by using 9.4× NEB buffer 2.1, 25 ng µl^{-1} guide RNA, 1.25 µM Lba Cas12a (NEB) and 4 µM fluorophore-quenched ssDNA fluorescent reporter (56-FAM/TTATT/3IABkFQ) (IDT). Cas reaction mix (2.5 µl) was added to each 50 µl RPA reaction mix and then again incubated for 10 min at 37 °C before continuous fluorescence readout in a Biotek Synergy NEO HTS plate reader for 150 min at 37 °C. During optimization, several reactions were run from a single RPA tube (using final volumes of 10, 12.5 or 25 µl instead of 50 µl); however, the same final concentrations of all reagents were conserved. Higher volumes and mixing of samples and RPA reactions improve sensitivity.

Tube-scale one-step Sherlock

CRISPR-based sensor reactions were prepared using 40 nM EnGen Lba Cas12a (NEB), 5,250 nM gRNA, 1× NEB buffer 2.1, 500 nM each of the RPA primers (IDT), 4 mM HEPES (4-(2-hydroxyethyl)-1-piperazineethanesulfonic acid) (pH 8.6) (Sigma-Aldrich), 12 mM NaCl (Sigma-Aldrich), 1% polyethylene glycol 8000 (Sigma-Aldrich), 1 µM fluorophore-quenched ssDNA fluorescent reporter (56-FAM/TTATT/3IABkFQ) (IDT), 14 mM magnesium acetate (TwistDx) and 1 TwistAmp Basic RPA pellet (TwistDx). Prepared sensor reactions excluding the magnesium acetate were deposited into 0.2-ml PCR tubes together with 10 µl of DNA at a given target concentration. Magnesium acetate was then added, and the reactions were incubated for 10 min at 37 °C before continuous fluorescence readout in a Biotek Synergy NEO HTS plate reader for 150 min at 37 °C.

Digital Sherlock (dSHERLOCK)

CRISPR-based sensor reactions were prepared as final concentrations of 40 nM EnGen Lba Cas12a (NEB), 5,250 nM gRNA, 1× NEB buffer 2.1, 500 nM each of the RPA primers (IDT), 4 mM Tris (tris(hydroxymethyl) aminomethane, pH 8.19) (Sigma-Aldrich), 12 mM NaCl (Sigma-Aldrich), 1% polyethylene glycol 35000 (Sigma-Aldrich), 0.01% Polysorbate 20, 1 µM fluorophore-quenched ssDNA fluorescent reporter (56-FAM/TTATT/3IABkFQ) (IDT), 14 mM magnesium acetate (TwistDx), 1 µM ROX reference dye (Invitrogen) and 1 TwistAmp Basic RPA pellet (TwistDx). From these reagents, two master mixes were prepared: an RPA mix (at 1.5× final concentrations, containing Tris (pH 8.19), NaCl, PEG 35 kDa, Polysorbate 20 and ROX reference dye) and a CAS mix (containing 6.77× final concentrations of Cas12a, gRNA, ssDNA fluorescent reporter and supplemental magnesium acetate). All reagents were prepared and kept on ice before mixing. Initially, 33.3 µl RPA mix was deposited onto each lyophilised TwistAmp Basic pellet before mixing and splitting into two separate tubes. To each tube, 5 µl sample or target DNA at a given concentration was added. The overall reaction was initiated by the addition of 3.75 µl CAS master mix, containing magnesium as a necessary enzymatic cofactor to activate both the Cas and RPA reaction, followed by immediate vortexing at medium speed for 5 s. The tubes were briefly spun down again and 14.5 µl were pipetted into the solution loading blade. To ensure consistency between samples, exactly 1 min after adding the Cas master mix, the solution was loaded into the QuantStudio 3D Digital PCR 20 K v2 Chip (Applied Biosystems) that was heated to 40 °C within 10 s. The bridging surface liquid was allowed to evaporate for 30 s before immersion fluid was applied, the chip lid was attached, and the cavity filled with immersion fluid (see Supplementary Fig. 1). Images were collected using a Hamamatsu ORCA-FLASH 4.0 CMOS camera (Model C11440-22C, Hamamatsu) on a Zeiss Axio Zoom V16 every 2 min for 2.5 h, with the first two images at room temperature and subsequent images at 37 °C. Temperature was controlled using a ThermoPlate TPi-SQPX (Tokai). In other experiments, images were collected every 10 min and for a total duration of up to 24 h. Reaction mix not used in the digital experiment was quantified as a tube-scale control using continuous fluorescence readout in a Biotek Synergy NEO HTS plate reader for 150 min at 37 °C.

dSHERLOCK *C. auris* calibration curve

The calibration curve was recorded in triplicate after 2.5 h of measurements with synthetic *C. auris* DNA containing the Internal Transcribed Spacer 2 gene. Target concentrations in samples were 500 aM, 1 fM, 5 fM, 50 fM, 500 fM and 1 pM in nuclease-free water. Partitions were evaluated as positive if their background-subtracted fluorescence crossed a threshold of 3,000 RFU. Error bars represent the standard deviation of three biological replicates. Background was calculated as the mean of three samples without DNA plus three times their standard deviation. The calibration curve was fit using a 4-parameter logistic regression, minimizing the sum of square errors. The limit of detection was calculated as the point where the fit curve intersects the background. Intervals between images were 2 min.

dSHERLOCK *FKS1* mutant calibration curve

The calibration curve was recorded in triplicate after 1 h of measurements with synthetic *FKS1* DNA containing the locus of the SNP mutation. Target concentrations in samples were 25 aM, 50 aM, 500 aM,

5 fM, 50 fM and 100 fM in nuclease-free water. Partitions were evaluated as positive if their background-subtracted fluorescence had crossed a threshold of 3,000 RFU. Error bars represent the standard deviation of three biological replicates. Background was calculated as the mean of three samples without DNA plus three times their standard deviation. The calibration curve was fit using a 4-parameter logistic regression, minimizing the sum of square errors. The limit of detection was estimated to be below the lowest measured concentration due to non-detectable background signal. Intervals between images were 2 min.

dSHERLOCK *FKS1* wild-type calibration curve

The calibration curve was recorded in triplicate after 2 h of measurements with synthetic *FKS1* DNA containing the wild-type locus of the SNP. Target concentrations in samples were 25 aM, 50 aM, 500 aM, 5 fM, 50 fM and 100 fM in nuclease-free water. Partitions were evaluated as positive if their background-subtracted fluorescence had crossed a threshold of 3,000 RFU. Error bars represent the standard deviation of three biological replicates. Background was calculated as the mean of three samples without DNA plus three times their standard deviation. The calibration curve was fit using a 4-parameter logistic regression, minimizing the sum of square errors. The limit of detection was calculated as the point where the fit curve intersects the background. Intervals between images were 10 min.

Guide RNA production

Single-stranded ultramers containing the guide sequence and a T7-promoter region, as well oligos complementary to the promoter were purchased from IDT. Ultramers and the oligos were annealed and the HiScribe T7 quick protocol (NEB) was used for gRNA transcription overnight at 37 °C. The product was treated with Dnase I (NEB), the RNA was purified with a Zymo Research RNA cleanup kit and then quantified using a nanodrop spectrophotometer (ThermoFisher).

Preparation of heat-killed simulated swab surveillance samples

Simulated swab samples were prepared from *C. auris* cultures. Isolates were streaked on Sabouraud dextrose agar (SDA) plates and incubated at 30 °C for 48 h. Subculture isolates were selected and incubated at 30 °C for ~24 h on SDA plates. Isolate identity was confirmed using MALDI-TOF-MS. Subculture isolates were diluted into PBS–BSA, concentration was adjusted to an optical density at 530 nm (OD_{530}) of 0.1 (80% T, 10^6 c.f.u.s ml^{-1} stock) and serially diluted in 10-fold increments to 10^3 c.f.u.s ml^{-1}. Stock (100 ml of 10^3 c.f.u.s ml^{-1}) was plated on SDA in duplicate and incubated at 30 °C for 48 h to confirm c.f.u. counts.

Simulated samples of 10^5 c.f.u.s ml^{-1} (high), 10^4 c.f.u.s ml^{-1} (moderate) and 10^3 c.f.u.s ml^{-1} (low) were prepared by aliquoting 100 ml of 10× cell suspension into 900 ml BD E-swab (Amies) medium (BD 220245, Copan Italia S.P.A.). Subsequently, simulated samples were heat inactivated by incubating at 90 °C in a water bath for 3 h. Sample concentrations were quantified in terms of fungal c.f.u.s ml^{-1} and a *C. auris* real-time qPCR assay[37] (BD Max System, Becton Dickinson).

Genomic DNA samples were heat inactivated by incubating at 70 °C in a water bath for 30 min, homogenized and extracted using QIAcube (Qiagen).

Preparation of heat-killed patient-derived surveillance samples

De-identified and residual composite surveillance samples (nares, axilla and groin swabs) in Amies media were obtained from the Wadsworth Center of the New York State Department of Health during September and October 2024 under Wadsworth Center IRB-exempt protocol 03-037. All swabs were tested by PCR (BD Max System) following Wadsworth Center protocols. A 100-µl aliquot of each sample was streaked onto ChromAgar Candida Plus and incubated at 37 °C for at least 2 days. MALDI-TOF-MS was used to confirm the identity of any single colony that appeared to be *C. auris* (pink with blue halo). For positive samples, the swab liquid was stored at 4 °C, while negative samples were initially stored at 4 °C before being transferred to −80 °C. The Wadsworth Center Laboratories selected 30 total samples: 3 high (C_t = ~20, ~10^5 c.f.u.s ml^{-1}), 3 moderate (C_t = ~23, ~10^4 c.f.u.s ml^{-1}), 3 low (C_t = ~26, ~10^3 c.f.u.s ml^{-1}) and 6 very low (C_t = ~29, ~10^2 c.f.u.s ml^{-1}, or C_t = ~32) samples for inclusion in the blinded panel and 15 PCR-negative swabs. All samples were heat killed by incubation in a water bath at 90 °C for 3 h, and sterility was confirmed by plating swab liquid on SDA plates.

ddPCR

The BioRad QX200 digital droplet PCR system in the Boston Children's Hospital Intellectual and Developmental Disabilities Research Center Molecular Genetics Core Facility was used, following manufacturer guidelines.

Computational methods: image processing

Reporter channel images were field-flatness corrected by dividing the image with the normalized pixel intensity from a homogeneously fluorescent green UV-resistant cast acrylic sheet (85635K411, McMaster-Carr). Individual microwells were identified using a fluorescence intensity threshold on the ROX channel. An approximate global threshold was determined using Yen's thresholding method[50], and multiple neighbouring thresholds were examined iteratively to account for local variations. At each threshold, appropriately sized connected components were retained to generate a mask that corresponded to filled microwells. To account for small movements of the chip between subsequent images, the locations of three microwells, evenly distributed on the chip along the *y* axis, were tracked and a Euclidean transformation was estimated. Inverse transformations were applied to all images, resulting in uniform orientation of the chip throughout time. To ensure robustness to environmental contamination, such as the settling of dust on the chip, the binary masks for each timepoint were multiplied, such that partitions that became unrecognizable over time were ignored. Coordinates of each microwell, as well as intensities in both the ROX channel and the FAM channel throughout time were extracted.

The master mask built on the ROX channel composite aligned stack was applied to all displacement-corrected images in the FAM reporter dye channel, and the average fluorescence intensity of pixels within individual compartments was extracted at each timepoint. To correct for background fluorescence, the initial fluorescence intensity of each microwell (recorded before powering the heater on) was subtracted from all subsequent images of the same microwell. A rationally chosen threshold was drawn to separate microwells with active reactions from those that did not detect target DNA. Target DNA concentration was calculated using Poisson statistics from the aggregate number of microwells with fluorescence intensity greater than the threshold.

Computational methods: timeseries processing

Fluorescence intensities were background corrected by subtracting the FAM intensity at time zero from all subsequent images of the same microwell. Trajectories, corresponding to the FAM fluorescence intensity as a function of time, were smoothed by applying a Gaussian-weighted, rolling average over three subsequent measurements. For thresholding-based evaluation, a microwell was counted as positive if at any point in time its background-corrected, smoothed FAM fluorescence intensity was greater than an appropriately chosen threshold.

Computational methods: feature extraction and dimensionality reduction

For the machine-learning-based classification of microwells containing different SNP alleles of a gene, features were extracted from the

background-corrected, Gaussian-smoothed FAM fluorescence intensity as a function of time. Reaction velocity was calculated as the difference between two measurements and divided by the interval between the measurements in minutes. Features extracted at an explicit timepoint were calculated in units of minutes, enabling the integration of datasets collected with different imaging time intervals. All features are described in Supplementary Table 6.

PCA was applied to eight continuous features described in Supplementary Table 6 using sci-kit learn with default parameters and numbers of components corresponding to the number of continuous features.

Computational methods: GRANITE

The Gaussian fitting algorithm was based on an initial estimation of a threshold value through fitting of a partial Gaussian and subsequent iterative improved fit to reliably label compartments as negative for DNA (Supplementary Fig. 11). GRANITE worked well for highly active batches in which the distributions of the compartments containing wild-type targets were clearly separated from those lacking DNA, but also for batches with very poor activity where two separate distributions were not clearly recognizable. Employing this method, we removed the negative compartments (that is, those lacking an active reaction) from the dataset, rather than keeping them as a third label for the supervised machine learning algorithm.

Computational methods: classification

Training data for the classifier were taken from chips containing templates of only a single allele that had been quantified for a minimum of 15 h, to ensure separation of positive and negative compartments in their maximum fluorescence values. The negatives class was labelled by fitting a Gaussian distribution to the microwells showing a maximum FAM fluorescence intensity below a rationally chosen threshold at the last available timepoint. All microwells with a maximum FAM fluorescence intensity above the mean of the Gaussian and with a probability $p < 10^{-5}$ of belonging to the Gaussian-distributed negative class were labelled as the respective positive allele class. These labels were used as ground truth to build the classifier.

To remove outliers, z-scores were calculated for both the initial ROX fluorescence intensity and the initial FAM fluorescence intensity for each chip. Microwells with a z-score >2.5 were removed from the training dataset. Microwells from the outer 5% of each edge were discarded to account for reaction variance from temperature gradients.

A random-forest classifier with 500 individual trees was trained on 14,000 reactions for each allele, obtained from 22 chips from experiments performed on 9 separate days. All timepoint-based features, PCs and underlying continuous features, as well as the ground-truth labels were used.

The classifier was tested on a holdout set of 1,000 trajectories for each allele, obtained from the same chips as the training data.

Reporting summary

Further information on research design is available in the Nature Portfolio Reporting Summary linked to this article.

Data availability

The data supporting the findings of this study are available within the paper and its Supplementary Information. Example data can be downloaded from figshare at https://doi.org/10.6084/m9.figshare.29944823 (ref. 51). Should any raw data files be needed in another format, they are available from the corresponding author on reasonable request.

Code availability

The image processing and machine learning scripts have been deposited in the open-access online repository GitHub and may be accessed at https://github.com/Walt-Lab/dSherlock (ref. 52). The source code is also available as a Code Ocean Compute Capsule at https://doi.org/10.24433/CO.6935105 (ref. 53). The image processing and machine learning scripts have been deposited in GitHub at https://github.com/Walt-Lab/dSherlock (ref. 52) and in Zenodo at https://doi.org/10.5281/zenodo.17153993 (ref. 54).

References

1. *WHO Fungal Priority Pathogens List to Guide Research, Development and Public Health Action* (World Health Organization, 2022).
2. Fisher, M. C. et al. Tackling the emerging threat of antifungal resistance to human health. *Nat. Rev. Microbiol.* **20**, 557–571 (2022).
3. *Antibiotic Resistance Threats in the United States 2019* (CDC, 2019).
4. Mishra, S. K., Yasir, M. & Willcox, M. *Candida auris*: an emerging antimicrobial-resistant organism with the highest level of concern. *Lancet Microbe* **4**, e482–e483 (2023).
5. Dennis, E. K., Chaturvedi, S. & Chaturvedi, V. So many diagnostic tests, so little time: review and preview of *Candida auris* testing in clinical and public health laboratories. *Front. Microbiol.* **12**, 757835 (2021).
6. Wickes, B. L. & Wiederhold, N. P. Molecular diagnostics in medical mycology. *Nat. Commun.* **9**, 5135 (2018).
7. Jeffery-Smith, A. et al. *Candida auris*: a review of the literature. *Clin. Microbiol. Rev.* **31**, e00029-17 (2017).
8. Satoh, K. et al. *Candida auris* sp. nov., a novel ascomycetous yeast isolated from the external ear canal of an inpatient in a Japanese hospital. *Microbiol. Immunol.* **53**, 41–44 (2009).
9. Spivak, E. S. & Hanson, K. E. *Candida auris*: an emerging fungal pathogen. *J. Clin. Microbiol.* **56**, e01588-17 (2018).
10. Zhang, S. X. et al. Recognition of diagnostic gaps for laboratory diagnosis of fungal diseases: expert opinion from the Fungal Diagnostics Laboratories Consortium (FDLC). *J. Clin. Microbiol.* **59**, e0178420 (2021).
11. Chen, J. S. et al. CRISPR-Cas12a target binding unleashes indiscriminate single-stranded DNase activity. *Science* **360**, 436–439 (2018).
12. Gootenberg, J. S. et al. Multiplexed and portable nucleic acid detection platform with Cas13, Cas12a, and Csm6. *Science* **360**, 439–444 (2018).
13. Gootenberg, J. S. et al. Nucleic acid detection with CRISPR-Cas13a/C2c2. *Science* **356**, 438–442 (2017).
14. Kaminski, M. M., Abudayyeh, O. O., Gootenberg, J. S., Zhang, F. & Collins, J. J. CRISPR-based diagnostics. *Nat. Biomed. Eng.* **5**, 643–656 (2021).
15. de Puig, H. et al. Minimally instrumented SHERLOCK (miSHERLOCK) for CRISPR-based point-of-care diagnosis of SARS-CoV-2 and emerging variants. *Sci. Adv.* **7**, eabh2944 (2021).
16. Nguyen, P. Q. et al. Wearable materials with embedded synthetic biology sensors for biomolecule detection. *Nat. Biotechnol.* **39**, 1366–1374 (2021).
17. Nguyen, L. T., Smith, B. M. & Jain, P. K. Enhancement of trans-cleavage activity of Cas12a with engineered crRNA enables amplified nucleic acid detection. *Nat. Commun.* **11**, 4906 (2020).
18. Ooi, K. H. et al. An engineered CRISPR-Cas12a variant and DNA-RNA hybrid guides enable robust and rapid COVID-19 testing. *Nat. Commun.* **12**, 1739 (2021).
19. Wang, Y. et al. Systematic evaluation of CRISPR-Cas systems reveals design principles for genome editing in human cells. *Genome Biol.* **19**, 62 (2018).
20. Huyke, D. A. et al. Enzyme kinetics and detector sensitivity determine limits of detection of amplification-free CRISPR-Cas12 and CRISPR-Cas13 diagnostics. *Anal. Chem.* **94**, 9826–9834 (2022).

21. Blanluet, C., Huyke, D. A., Ramachandran, A., Avaro, A. S. & Santiago, J. G. Detection and discrimination of single nucleotide polymorphisms by quantification of CRISPR-Cas catalytic efficiency. *Anal. Chem.* **94**, 15117–15123 (2022).
22. Athamanolap, P. et al. Nanoarray digital polymerase chain reaction with high-resolution melt for enabling broad bacteria identification and pheno-molecular antimicrobial susceptibility test. *Anal. Chem.* **91**, 12784–12792 (2019).
23. Luo, Y. et al. SAMBA: a multicolor digital melting PCR platform for rapid microbiome profiling. *Small Methods* **6**, 2200185 (2022).
24. Miglietta, L. et al. Adaptive filtering framework to remove nonspecific and low-efficiency reactions in multiplex digital PCR based on sigmoidal trends. *Anal. Chem.* **94**, 14159–14168 (2022).
25. Moniri, A., Miglietta, L., Holmes, A., Georgiou, P. & Rodriguez-Manzano, J. High-level multiplexing in digital PCR with intercalating dyes by coupling real-time kinetics and melting curve analysis. *Anal. Chem.* **92**, 14181–14188 (2020).
26. Rolando, J. C., Jue, E., Schoepp, N. G. & Ismagilov, R. F. Real-time, digital LAMP with commercial microfluidic chips reveals the interplay of efficiency, speed, and background amplification as a function of reaction temperature and time. *Anal. Chem.* **91**, 1034–1042 (2019).
27. Schoepp, N. G. et al. Rapid pathogen-specific phenotypic antibiotic susceptibility testing using digital LAMP quantification in clinical samples. *Sci. Transl. Med.* **9**, eaal3693 (2017).
28. Shinoda, H. et al. Amplification-free RNA detection with CRISPR–Cas13. *Commun. Biol.* **4**, 476 (2021).
29. Tian, T. et al. An ultralocalized Cas13a assay enables universal and nucleic acid amplification-free single-molecule RNA diagnostics. *ACS Nano* **15**, 1167–1178 (2021).
30. Yue, H. et al. Droplet Cas12a assay enables DNA quantification from unamplified samples at the single-molecule level. *Nano Lett.* **21**, 4643–4653 (2021).
31. Roh, Y. H. et al. CRISPR-enhanced hydrogel microparticles for multiplexed detection of nucleic acids. *Adv. Sci.* **10**, 2206872 (2023).
32. Shinoda, H. et al. Automated amplification-free digital RNA detection platform for rapid and sensitive SARS-CoV-2 diagnosis. *Commun. Biol.* **5**, 473 (2022).
33. Park, J. S. et al. Digital CRISPR/Cas-assisted assay for rapid and sensitive detection of SARS-CoV-2. *Adv. Sci.* **8**, 2003564 (2021).
34. Wu, X. et al. Digital CRISPR-based method for the rapid detection and absolute quantification of nucleic acids. *Biomaterials* **274**, 120876 (2021).
35. Yu, Z., Xu, L., Lyu, W. & Shen, F. Parallel multistep digital analysis SlipChip demonstrated with the quantification of nucleic acid by digital LAMP-CRISPR. *Lab Chip* **22**, 2954–2961 (2022).
36. Kordalewska, M. et al. Rapid and accurate molecular identification of the emerging multidrug-resistant pathogen *Candida auris*. *J. Clin. Microbiol.* **55**, 2445–2452 (2017).
37. Leach, L., Zhu, Y. & Chaturvedi, S. Development and validation of a real-time PCR assay for rapid detection of *Candida auris* from surveillance samples. *J. Clin. Microbiol.* **56**, e01223-17 (2018).
38. Denancé, N., Briand, M., Gaborieau, R., Gaillard, S. & Jacques, M.-A. Identification of genetic relationships and subspecies signatures in *Xylella fastidiosa*. *BMC Genomics* **20**, 239 (2019).
39. *Procedure for Collection of Patient Swabs for Candida auris* (Centers for Disease Control and Prevention, 2022).
40. Zhu, Y. et al. Laboratory analysis of an outbreak of *Candida auris* in New York from 2016 to 2018: impact and lessons learned. *J. Clin. Microbiol.* **58**, e01503-19 (2020).
41. Kellner, M. J., Koob, J. G., Gootenberg, J. S., Abudayyeh, O. O. & Zhang, F. SHERLOCK: nucleic acid detection with CRISPR nucleases. *Nat. Protoc.* **14**, 2986–3012 (2019).
42. Rolando, J. C., Jue, E., Barlow, J. T. & Ismagilov, R. F. Real-time kinetics and high-resolution melt curves in single-molecule digital LAMP to differentiate and study specific and non-specific amplification. *Nucleic Acids Res.* **48**, e42 (2020).
43. Yao, Z. et al. Tuning the dynamic reaction balance of CRISPR/Cas12a and RPA in one pot: a key to switch nucleic acid quantification. *ACS Sens.* **9**, 3511–3519 (2024).
44. Kordalewska, M. et al. Understanding echinocandin resistance in the emerging pathogen *Candida auris*. *Antimicrob. Agents Chemother.* **62**, e00238-18 (2018).
45. *Reference Method for Broth Dilution Antifungal Susceptibility Testing of Yeasts* CLSI M27 (CLSI, 2017).
46. Wasylyshyn, A. & Stoneman, E. K. Management of *Candida auris*. *JAMA* **331**, 611–612 (2024).
47. Berkow, E. L., Lockhart, S. R. & Ostrosky-Zeichner, L. Antifungal susceptibility testing: current approaches. *Clin. Microbiol. Rev.* **33**, e00069-19 (2020).
48. Duvallet, C. et al. Nationwide trends in COVID-19 cases and SARS-CoV-2 RNA wastewater concentrations in the United States. *ACS ES T Water* **2**, 1899–1909 (2022).
49. *Addressing Foodborne Threats to Health: Policies, Practices, and Global Coordination: Workshop Summary* (National Academies Press, 2006).
50. Jui-Cheng, Y., Fu-Juay, C. & Shyang, C. A new criterion for automatic multilevel thresholding. *IEEE Trans. Image Process.* **4**, 370–378 (1995).
51. Rolando, J. C. et al. Example data for running the dSHERLOCK data analysis pipeline. *figshare* https://doi.org/10.6084/m9.figshare.29944823 (2025).
52. Rolando, J. C. et al. dSHERLOCK repository. *GitHub* https://github.com/Walt-Lab/dSherlock (2025).
53. Rolando, J. C. et al. dSHERLOCK compute capsule. *Code Ocean* https://doi.org/10.24433/CO.6935105 (2025).
54. Rolando, J. C. et al. Digital CRISPR-based diagnostics for quantification of *Candida auris* and resistance mutations. Source Code. *Zenodo* https://doi.org/10.5281/zenodo.17153993 (2025).

Acknowledgements

Digital Droplet PCR measurements were performed by the Boston Children's Hospital Intellectual and Developmental Disabilities Research Center Molecular Genetics Core Facility. The research described in this manuscript was supported by grants from The Wyss Institute for Bioinspired Engineering (J.C.R., A.T., D.R.W.), Health Research Inc. (GR110013801, N.E.W., N.K., H.d.P., X.T., J.J.C.), the New York State Department of Health, and the Wadsworth Center Division of Infectious Diseases (WC-2019-01, N.E.W., N.K., H.d.P., X.T., J.J.C.). N.K. was supported by the Wyss Technology Development Fellowship. X.T. acknowledges funding from the NIH NIDDK (5K08DK132516).

Author contributions

J.C.R, A.T. and N.E.W. conceived the technology, designed and conducted experiments, analysed results and prepared the manuscript. N.K. participated in study design, conducted experimental work, contributed to data analysis and provided materials essential to the study. H.d.P. and X.T. submitted the initial proposal and performed computational primer analyses. H.d.P. designed gRNA sequences and primers, conducted initial experiments and analysed the resulting data. E.C. prepared simulated swab samples, collected residual clinical composite surveillance swabs and characterized their molecular properties. V.C. helped design initial experiments, data analysis and interpretations. J.J.C. and D.R.W. jointly supervised the research. All authors reviewed and approved the final manuscript.

Competing interests

J.J.C. and D.R.W. had financial interests in and served on the board of Sherlock Biosciences Corporation, a company that develops CRISPR diagnostics; Sherlock Biosciences was acquired by OraSure Technologies. D.R.W.'s interests are reviewed and managed by Mass General Brigham and Harvard University in accordance with their conflict-of-interest policies. Harvard College and Brigham and Women's Hospital have filed Provisional Patent 63/764,169, on behalf of J.C.R., A.T. and D.R.W. related to the multiplexed single-molecule CRISPR detection described in this manuscript. The remaining authors declare no competing interests.

Additional information

Supplementary information The online version contains supplementary material available at https://doi.org/10.1038/s41551-025-01597-0.

Correspondence and requests for materials should be addressed to James J. Collins or David R. Walt.

Peer review information *Nature Biomedical Engineering* thanks Ruijie Dengvand, Tony Hu and the other, anonymous, reviewer(s) for their contribution to the peer review of this work. Peer reviewer reports are available.

Reprints and permissions information is available at www.nature.com/reprints.

Publisher's note Springer Nature remains neutral with regard to jurisdictional claims in published maps and institutional affiliations.

Springer Nature or its licensor (e.g. a society or other partner) holds exclusive rights to this article under a publishing agreement with the author(s) or other rightsholder(s); author self-archiving of the accepted manuscript version of this article is solely governed by the terms of such publishing agreement and applicable law.

© The Author(s), under exclusive licence to Springer Nature Limited 2026

[1]Department of Pathology, Brigham and Women's Hospital, Boston, MA, USA. [2]Wyss Institute for Biologically Inspired Engineering, Harvard University, Boston, MA, USA. [3]Harvard Medical School, Boston, MA, USA. [4]Institute for Medical Engineering and Science, Department of Biological Engineering, and Synthetic Biology Center, Massachusetts Institute of Technology, Cambridge, MA, USA. [5]Broad Institute of MIT and Harvard, Cambridge, MA, USA. [6]Division of Gastroenterology, Massachusetts General Hospital, Boston, MA, USA. [7]Wadsworth Center Mycology Lab, New York State Department of Health, Albany, NY, USA. [8]Department of Biological Engineering, Massachusetts Institute of Technology, Cambridge, MA, USA. [9]Present address: Department of Chemical Engineering and Applied Chemistry, Institute for Studies in Transdisciplinary Engineering Education and Practice, University of Toronto, Toronto, Ontario, Canada. [10]Present address: Westchester Medical Center/New York Medical College, Valhalla, NY, USA. [11]These authors contributed equally: Justin C. Rolando, Anton Thieme, Nicole E. Weckman. [12]These authors jointly supervised this work: James J. Collins, David R. Walt. ✉e-mail: jimjc@mit.edu; dwalt@bwh.harvard.edu

nature portfolio

Corresponding author(s): JJ Collins, DR Walt

Last updated by author(s): 2025/9/22

Reporting Summary

Nature Portfolio wishes to improve the reproducibility of the work that we publish. This form provides structure for consistency and transparency in reporting. For further information on Nature Portfolio policies, see our Editorial Policies and the Editorial Policy Checklist.

Statistics

For all statistical analyses, confirm that the following items are present in the figure legend, table legend, main text, or Methods section.

n/a	Confirmed	
☐	☒	The exact sample size (*n*) for each experimental group/condition, given as a discrete number and unit of measurement
☐	☒	A statement on whether measurements were taken from distinct samples or whether the same sample was measured repeatedly
☐	☒	The statistical test(s) used AND whether they are one- or two-sided *Only common tests should be described solely by name; describe more complex techniques in the Methods section.*
☒	☐	A description of all covariates tested
☐	☒	A description of any assumptions or corrections, such as tests of normality and adjustment for multiple comparisons
☐	☒	A full description of the statistical parameters including central tendency (e.g. means) or other basic estimates (e.g. regression coefficient) AND variation (e.g. standard deviation) or associated estimates of uncertainty (e.g. confidence intervals)
☐	☒	For null hypothesis testing, the test statistic (e.g. *F*, *t*, *r*) with confidence intervals, effect sizes, degrees of freedom and *P* value noted *Give P values as exact values whenever suitable.*
☒	☐	For Bayesian analysis, information on the choice of priors and Markov chain Monte Carlo settings
☒	☐	For hierarchical and complex designs, identification of the appropriate level for tests and full reporting of outcomes
☐	☒	Estimates of effect sizes (e.g. Cohen's *d*, Pearson's *r*), indicating how they were calculated

Our web collection on statistics for biologists contains articles on many of the points above.

Software and code

Policy information about availability of computer code

Data collection	Images were collected using the commercially available software Zeiss Zen Blue Edition.

Data analysis	For this study, custom python code was developed to perform the following components of the data analysis: 1. extraction of fluorescence time series within individual partitions on the chip from microscopy images 2. extraction of features describing the kinetics of the reactions from the fluorescence time series 3. training of a classifier based on the features 4. estimation of analyte concentrations based on a feature (threshold) or the output of a classifier The Python code is submitted with the manuscript using the platform Code Ocean (DOI: 10.24433/CO.6935105) and GitHub (https://github.com/Walt-Lab/dSherlock). These include examples of use in the form of interactive Jupyter notebooks with example data for all aspects of the data analysis except the training of a classifier. A Jupyter notebook illustrating the training of a classifier is included but is not executable due to constraints in the size of example data. The python code uses python 3.9.19 and most notable relies on the following python libraries: scikit-image=0.24.0 scikit-learn=1.1.3 pandas=2.2.2 A full list of libraries and versions used can be found in the environment.yml file on Code Ocean Compute Capsule under DOI 10.24433/CO.6935105.

For manuscripts utilizing custom algorithms or software that are central to the research but not yet described in published literature, software must be made available to editors and reviewers. We strongly encourage code deposition in a community repository (e.g. GitHub). See the Nature Portfolio guidelines for submitting code & software for further information.

Data

Policy information about availability of data

All manuscripts must include a data availability statement. This statement should provide the following information, where applicable:

- Accession codes, unique identifiers, or web links for publicly available datasets
- A description of any restrictions on data availability
- For clinical datasets or third party data, please ensure that the statement adheres to our policy

The data supporting the findings of this study are available within the paper and Supplemenary Information files. Should any raw data files be needed in another format they are available from the corresponding author upon reasonable request. Example data can be downloaded from figshare with the following DOI: 10.6084/m9.figshare.29944823. The Python code is submitted with the manuscript using the platform Code Ocean (DOI: 10.24433/CO.6935105) and GitHub (https://github.com/Walt-Lab/dSherlock; DOI: 10.5281/zenodo.17153993).

Research involving human participants, their data, or biological material

Policy information about studies with human participants or human data. See also policy information about sex, gender (identity/presentation), and sexual orientation and race, ethnicity and racism.

Reporting on sex and gender	N/A
Reporting on race, ethnicity, or other socially relevant groupings	N/A
Population characteristics	De-identified and residual composite surveillance samples (nares, axilla, and groin swabs) in Amies media were obtained from the Wadsworth Center of the New York State Department of Health during September and October 2024 under Wadsworth Center IRB-exempt protocol 03-037. These specimens were provided solely for assay development purposes and were not collected under a protocol involving human subject participation. Accordingly, this work was classified as Not Human Subjects Research. The assays were not validated for safety, efficacy, or effectiveness.
Recruitment	All clinical samples were de-identified and provided without any protected identifying health information.
Ethics oversight	Study protocols were reviewed by Wadsworth Center IRB-exempt protocol 03-037 and the Harvard Institutional Biosafety Committee.

Note that full information on the approval of the study protocol must also be provided in the manuscript.

Field-specific reporting

Please select the one below that is the best fit for your research. If you are not sure, read the appropriate sections before making your selection.

☒ Life sciences ☐ Behavioural & social sciences ☐ Ecological, evolutionary & environmental sciences

For a reference copy of the document with all sections, see nature.com/documents/nr-reporting-summary-flat.pdf

Life sciences study design

All studies must disclose on these points even when the disclosure is negative.

Sample size	Sample sizes for experiments were three or greater. For digital experiments, individual samples were broken into approximately 20,000 compartments. No sample size calculation for composite surveillance swabs was performed; 15 and 30 representative surveillance samples were selected by the Wadsworth Center of the New York State Department of Health.
Data exclusions	No collected data were excluded from analysis. We did not process images of chips with broken sections due to manufacturing defects.
Replication	Experiments were performed as three or greater replicates. All attempts at replication are described in the manuscript and no data were excluded.
Randomization	Not relevant to this study.
Blinding	Investigators performing dSHERLOCK were blinded to the sample identity of the clinical isolates in 2c and 3fgh. After submitting quantification results, investigators were unblinded by Wadsworth Center of the New York State Department of Health, who prepared the panels.

Reporting for specific materials, systems and methods

We require information from authors about some types of materials, experimental systems and methods used in many studies. Here, indicate whether each material, system or method listed is relevant to your study. If you are not sure if a list item applies to your research, read the appropriate section before selecting a response.

Materials & experimental systems

n/a	Involved in the study
☒	☐ Antibodies
☐	☒ Eukaryotic cell lines
☒	☐ Palaeontology and archaeology
☐	☒ Animals and other organisms
☒	☐ Clinical data
☒	☐ Dual use research of concern
☒	☐ Plants

Methods

n/a	Involved in the study
☒	☐ ChIP-seq
☒	☐ Flow cytometry
☒	☐ MRI-based neuroimaging

Eukaryotic cell lines

Policy information about cell lines and Sex and Gender in Research

Cell line source(s)	HEK293FT cells were obtained from Invitrogen (catalog #R70007).
Authentication	The cell line was not independently authenticated.
Mycoplasma contamination	Cultures were tested for mycoplasma contamination using a commercial kit (Lonza MycoAlert, #LT07-318) and were confirmed negative.
Commonly misidentified lines (See ICLAC register)	No commonly misidentified cell lines were used in this study.

Animals and other research organisms

Policy information about studies involving animals; ARRIVE guidelines recommended for reporting animal research, and Sex and Gender in Research

Laboratory animals	N/A
Wild animals	N/A
Reporting on sex	N/A
Field-collected samples	Simulated swab samples were prepared from cultured isolates. Isolates were streaked on Sabouraud dextrose agar (SDA) plates and incubated at 30 °C for 48h. Subculture isolates were selected and incubated at 30 °C for ~24h on SDA plates. Isolate identity was confirmed using MALDI. Subculture isolates were diluted into PBS-BSA, concentration adjusted to an OD530 = 0.1 (80% T, 106 CFU/mL stock), and serially diluted in ten-fold increments to 10^3 CFU/mL. 100 mL of 10^3 CFU/mL stock was plated on SDA in duplicate and incubated at 30 °C for 48h to confirm CFU counts.

Simulated samples of 10^5 CFU/mL (high), 10^4 CFU/mL (moderate), and 10^3 CFU/mL (low) were prepared by aliquoting 100 mL of 10x cell suspension into 900 mL BD E-swab (Amies) medium (BD 220245, Copan Italia S.P.A, Brescia, Italy). Subsequently, simulated samples were heat-inactivated by incubating at 90 °C in a water bath for 3h. Sample concentrations were verified using real-time PCR (BD Max System; Becton, Dickinson and Company, Franklin Lakes, NJ).

Preparation of heat-killed patient-derived surveillance samples
Nares/axilla/groin swabs were collected from patients in September and October of 2024 in Amies media. All swabs were tested by PCR (BD Max System) following Wadsworth Center protocols. A 100 µL aliquot of each sample was streaked onto ChromAgar Candida Plus and incubated at 37 ºC for at least two days. MALDI-TOF-MS was use to confirm the identity of any single colony that appeared to be C. auris (pink with blue halo). For positive samples, the swab liquid was stored at 4 ºC, while negative samples were initially stored at 4 ºC before being transferred to –80 ºC. The Wadsworth Center Laboratories selected 30 total samples for inclusion in the blinded panel: 3 high (CT = ~20, ~10^5 CFU/mL), 3 moderate (CT = ~23, ~10^4 CFU/mL), 3 low (CT = ~26, ~10^3 CFU/mL), and 6 very low (CT = ~29, ~10^2 CFU/mL) or (CT = ~32) samples for inclusion in the blinded panel and 15 PCR-negative swabs. All samples were heat-killed by incubation in a water bath at 90 ºC for 3 hours, and the sterility confirmed by plating swab liquid on Sabouraud dextrose agar (SDA) plates.

Ethics oversight

Study protocols were reviewed by the Harvard Institutional Biosafety Committee.

Note that full information on the approval of the study protocol must also be provided in the manuscript.

Plants

Seed stocks

N/A

Novel plant genotypes

N/A

Authentication

N/A